Blindness affects the developmental trajectory of the sleeping brain

Helene Vitali [a,b], Claudio Campus [a], Sabrina Signorini [c], Valentina De Giorgis [c,d,e], Federica Morelli [c,d], Costanza Varesio [c,d,e], Ludovica Pasca [c,d,e], Alessia Sammartano [c,e], Monica Gori [a,*]

[a] Unit for Visually Impaired People, Center for Human Technologies, Fondazione Istituto Italiano di Tecnologia, Istituto Italiano di Tecnologia, Via Enrico Melen 83, Building B, Genoa 16152, Italy
[b] DIBRIS, University of Genova, Genoa 16145, Italy
[c] Department of Child Neurology and Psychiatry, IRCCS Mondino Foundation, Pavia 27100, Italy
[d] Department of Brain and Behavioural Sciences, University of Pavia, Pavia 27100, Italy
[e] Member of European Reference Network for Rare and Complex Epilepsies, EpiCARE, Italy

ARTICLE INFO

ABSTRACT

Sleep plays a crucial role in brain development, sensory information processing, and consolidation. Sleep spindles are markers of these mechanisms as they mirror the activity of the thalamocortical circuits. Spindles can be subdivided into two groups, slow (10–13 Hz) and fast (13–16 Hz), which are each associated with different functions. Specifically, fast spindles oscillate in the high-sigma band and are associated with sensorimotor processing, which is affected by visual deprivation. However, how blindness influences spindle development has not yet been investigated. We recorded nap video-EEG of 50 blind/severely visually impaired (BSI) and 64 sighted children aged 5 months to 6 years old. We considered aspects of both macro- and micro-structural spindles. The BSI children lacked the evolution of developmental spindles within the central area. Specifically, young BSI children presented low central high-sigma and high-beta (25–30 Hz) event-related spectral perturbation and showed no signs of maturational decrease. High-sigma and high-beta activity in the BSI group correlated with clinical indices predicting perceptual and motor disorders. Our findings suggest that fast spindles are pivotal biomarkers for identifying an early developmental deviation in BSI children. These findings are critical for initial therapeutic intervention.

1. Introduction

From birth, sleep enhances brain development (Fifer et al., 2010; Grigg-Damberger, 2017; Miller et al., 2015; Sadeh et al., 2002). During sleep, the sensory information people have acquired while awake is reprocessed and consolidated (Fernandez and Lüthi, 2020; Fogel and Smith, 2011; Gruber and Wise, 2016). Sleep spindles are a marker of these mechanisms as they mirror the activity of the thalamocortical circuits, which are composed of neurons that integrate sensory and motor inputs (Fernandez and Lüthi, 2020; Halassa and Kastner, 2017; Steriade, 1999; Steriade et al., 1985) and undergo important changes in the first years of life (D'Atri et al., 2018; Kwon et al., 2023). Spindles are bursts of neural activity that oscillate in the sigma band (Fernandez and Lüthi, 2020; Steriade, 1999; Steriade et al., 1985), which is modulated by sleep to support visual plasticity (Aton et al., 2013; Menicucci et al.,

2022). This suggests that the absence of vision from birth could influence the maturation of sleep spindles. Therefore, we hypothesized that blindness may elicit a plastic reorganization of the brain structures that are involved in sleep processes.

Specifically, sleep spindles can be subdivided into two groups, slow and fast. Slow spindles oscillate in the low-sigma band (10–13 Hz) and prevail in the frontal area (Chatburn et al., 2013; Clemens et al., 2005; Doucette et al., 2015; Gruber et al., 2013; Hoedlmoser et al., 2014; Kurdziel et al., 2013; Tarokh et al., 2014). In turn, fast-spindles oscillate in the high-sigma band (13–16 Hz) and prevail in the central area (Barakat et al., 2011; Chatburn et al., 2013; Jaramillo et al., 2023; Schabus et al., 2007; Tamaki et al., 2008). Slow and fast spindles evolve with age in a manner that may reflect the maturation of the different sub-networks. Indeed, they present different evolutional processes during development (D'Atri et al., 2018; McClain et al., 2016; Ricci et al.,

2021; Shinomiya et al., 1999) that can be attributed to the existence of multiple generators (Shinomiya et al., 1999). Specifically, the higher frequencies increase through a child's first 6 months, while the slower rhythms become significantly less common across the same period (Louis et al., 1992). From age 1, and at least until reaching the 4-year mark, the slow spindles reverse this tendency and increase in density (D'Atri et al., 2018) while the fast spindles decrease in density (D'Atri et al., 2018; Page et al., 2018). Afterward, fast spindles linearly increase until adolescence, while slow spindles decline and show a following increase in early adolescence (Campbell and Feinberg, 2016; Shinomiya et al., 1999). These changes agree with the spindle frequency evolution described in a recent article that illustrates spindle characteristics from birth to 18 years of age (Kwon et al., 2023).

The spindles sub-groups are also associated with different functional skills: slow spindles are associated with high-level cognitive functions (e.g., intelligence and declarative learning), (Chatburn et al., 2013; Clemens et al., 2005; Doucette et al., 2015; Gruber et al., 2013; Hoedl-moser et al., 2014; Kurdziel et al., 2013; Tarokh et al., 2014). In turn, fast spindles are associated with sensorimotor processing (e.g., visuo-motor performance, motor functioning, and motor learning), which is affected by visual deprivation (Barakat et al., 2011; Chatburn et al., 2013; Jaramillo et al., 2023; Schabus et al., 2007; Tamaki et al., 2008). Indeed, vision plays a crucial role in the way our brains represent the body and the external world, and its absence alters the development of people's spatial, social and motor abilities (Rigato et al., 2014; Bollini et al., 2023; Cappagli et al., 2019, 2017; Gori et al., 2021; Cappagli et al., 2017; Houwen et al., 2007; Cappagli et al., 2019; Houwen et al., 2007, 2009). Therefore, given the strong association with sensorimotor pro-cessing, we hypothesized that fast spindle development may be specif-ically impacted in blind children.

To investigate our hypothesis, we recorded nap video-EEG in 50 blind or severely visually impaired (BSI) children and 64 sighted (S) children aged 5 months to 6 years old. We explored both macro- and micro-structural aspects. Specifically, we focused on three potential spindle biomarkers and their associations with clinical indices: the spatial spindle-frequency distribution on the scalp, spindles character-istics (density and duration), and spindles' event-related spectral perturbation (ERSP) after spindle onset in the different ROIs.

2. Materials and methods

2.1. Participants

114 children participated in the study; 50 were blind or visually impaired (BSI) and 64 were sighted (S). Both groups were subdivided into two age-bins in accordance with previous literature (Campus et al., 2021; McClain et al., 2016): the first bin included children from 5 months to less than 3 years and had 27 BSI subjects (13 Females, mean age = 1.65, sd=0.71) and 28 S subjects (13 Females, mean age = 1.58, sd=0.80); subsequently, the second bin had children from 3 to 6 years and included 23 BSI (16 Females, mean age = 4.46, sd=0.85) and 36 S (12 Females, mean age = 4.40, sd=0.87). We performed a *t*-test between the ages of the BSI and S groups for each age-bin. They were non-significant for both the 0–3 (t(53)=0.36, P = 0.72, 95 % CI=[−0.34, 0.48]y) and the 3–6 (t(57)=0.30, P = 0.80, 95 % CI=[−0.40, 0.52]y) age-bins. A histogram of age distribution and the exact age of each participant is reported in the supplementary materials (see Fig. S1). However, considering the maturational changes known to happen in the first decade of life, like cortical rewiring, we also counted age as a continuous predictor and found results that supported the adopted age-bin subdivision.

2.2. Ethics statement

We have complied with all relevant ethical regulations, and we have received informed consent from the participants' parents to use their instrumental and clinical data for research according to the guidelines of the Declaration of Helsinki.

2.3. Clinical details of the blind/visually impaired participants

Full clinical details are provided in Table S1 (see Supplemental In-formation). In this study, we enrolled children affected by congenital peripheral visual impairments (i.e., involving pre-chiasmatic structures, such as the retina and optic nerve) that were referred to the centre of Child Neurophthalmology of the IRCCS Mondino Foundation based in Pavia, Italy. Subjects with primary brain involvement (e.g., cerebral visual impairment) were excluded based on diverse criteria including medical history, clinical evaluations (neurologic and visual function assessments), and diagnostic exams (VEP, brain MRI, EEG). None of the participating children had a history of perinatal problems (such as res-piratory distress during delivery or suffering from an anoxic-ischemic-hemorrhagic injury), metabolic disorders, genetic syndromes, epi-lepsy, or sleep disorders. Only 4 children were born preterm. All 4 in this group were born late preterm and they had no neurological involve-ment. All the subjects had good general health. Some subjects presented a slight and nonspecific developmental delay (which is frequently re-ported in visually impaired infants) (Dale et al., 2017). However, based on the standardized evaluation, no children had cognitive impairment.

Developmental and cognitive assessments were performed using a comprehensive approach that included a multidisciplinary clinical evaluation and standardized tests that were chosen according to the participant's age and the severity of their blindness. These assessments were performed by trained professionals with expertise in evaluating blind and visually impaired children. The cognitive levels of this pop-ulation were evaluated using the verbal subscales of the Wechsler scales (Wechsler, 2003). Their developmental levels were assessed using the Reynell-Zinkin Scale (RZS) (Reynell, 1978). The RZS is a standardized developmental assessment test designed for children with disorders of the visual system. In turn, specific subscales of the RZS were selected as parameters to consider in the associated analysis (see the statistical analysis sections). Visual function evaluations were carried out by trained professionals. According to the age and cooperation level of the children, their grating or visual impairment was measured using stan-dardized tests. Infants were evaluated using the preferential look tech-nique (i.e., observing the child's spontaneous behaviors when facing a grating target (Hyvarinen et al., 1980)). Subsequently, the older chil-dren were administered either the Snellen Chart (Azzam and Ronquillo, 2023) or the LEA Vision Test (Hyvarinen et al., 1980) at a distance of 3 m, depending on their age and academic levels. The level of grating or visual acuity was graded based on the severity of the participants' visual deficits; these ranged from severe visual impairment to total blindness. Similarly, none of the participating children in the control group had a history of perinatal problems, metabolic disorders, genetic syndromes, epilepsy, diagnosed sleep disorders, or cognitive impairment.

2.4. Apparatus and materials

Daytime naps were recorded in the EEG lab of the Child Neuropsy-chiatrists Unit at the IRCCS Mondino Foundation Hospital, Pavia (Italy) with a 512 Hz sampling frequency using a Nicolet vEEG 5.94 system. The recordings included EEGs from 19 derivations (FP1, FP2, Fz, F3, F4, F7, F8, Cz, C3, C4, Pz, P3, P4, O1, O2, T3, T4, T5, T6) following the International 10–20 System. Further polygraphic channels included ECG, pneumogram (PNG), EMG, and electrooculogram (EOG), depending on the subject's compliance. Video was also acquired using two infrared cameras.

2.5. Procedure

Along with their parents (or legal guardians), the participants arrived at the laboratory at their scheduled time. Most of these

assessments occurred between 9 and 11 am. However, some participants came to the laboratory in the early afternoon (around 1 pm), due to familial difficulties. To verify that the diurnal and homeostatic dynamics did not influence our results, we tried to add the period of the day in which the nap was scheduled (morning vs. afternoon) as an independent variable in our models, which considered the spindles characteristics or power as the dependent variables. However, we found no significant interaction with the period of the day (the probability closest to significance was $P = 0.12$).

An expert EEG technician explained to the parents what the exam was about. Subsequently, they signed the informed consent form for the video-EEG recording and the use of data for research purposes. Then, the EEG cap was put on the participants and the polygraphic parameters were set. A band pass filter was set at 5–15 Hz for ECG, 0.5–5 Hz for PNG and EOG, and 50–70 Hz for EMG. The participants were placed in a dark, silent, and comfortable room, while an expert EEG technician continuously monitored their state. Starting from the first drowsiness period that appears on the EEG trace, the participant had 50 min of sleep possibility. The effective mean total sleep time (TST) and SE for each group and age-bin is outlined in Table S2. At the end of the 50 min or after the natural awakening of the child, the test finished, and the test material worn was disassembled. Sleep scoring (operated by two sleep experts) and the pre-processing analysis were performed offline. The study included the results of the participants who achieved at least 30 min of TST and N3 sleep stage.

2.6. Sleep scoring and pre-processing

The sleep recordings were processed using *EEGLAB* (Grandchamp and Delorme, 2011) and Hume (https://github.com/jsaletin/hume) software. Any missing or artifacted electrodes were interpolated. The EEG was filtered using a notch (50+−5 Hz) and a band-pass filter between 0.16 and 100 Hz; in turn, it was subsampled to 256 Hz and re-referenced to the average of all the electrodes. Data were scored for sleep stages using 30-s epochs, in accordance with the American Academy of Sleep Medicine manual criteria (Berry et al., 2020). The artifacts related to ocular, muscle, and cardiac activities, or related to problems with the electrodes were removed using a visually-inspected independent component analysis (ICA).

2.6.1. Sleep macrostructure

To compute the spectrogram, each scoring page was divided into 6 non-overlapping 5-s segments. Subsequently, on each segment, the power spectral density (PSD) was computed using the *pwelch* function (the window length was set to 5 s without overlap – as a default of Hume toolbox – and the nfft was set to 256, equal to the sampling frequency). Then, the mean PSD was computed by averaging all the segments within each 30-s epoch. For each 30-s epoch, the power of the sigma and delta frequency bands was calculated. The band power was then normalized to the mean power of all total sleep time (TST) according to the formula:

$$Normalized\ power\ (epoch) = \frac{power\ (epoch)}{mean\ (power\ of\ TST)} * 100 \qquad (1)$$

2.6.2. Sleep microstructure: spindle characteristics

The *detect spindles EEGLAB* plug-in (Ray et al., 2015) was used to automatically detect the sleep spindles (10–16 Hz) using a minimum duration threshold of 0.5 s. Fig. S2 shows a representative plot that includes EEG traces and marked detections. We considered spindle events on the Frontal (F3, F4, Fz) and Central (C3, C4, Cz) electrodes during the N2 and N3 sleep stages. The detections were inspected visually.

2.6.3. Sleep microstructure: spindle ERSP

To compute the event-related spectral perturbation (ERSP) in dB, the data were segmented from 1 s before to 4 s after the spindle onset (considered as $t = 0$). For each segment, the period from $−1$ s to 0 s was used as a baseline. In turn, ERSP was calculated using the *newtimef* function of EEGLAB. For each participant, the whole time-frequency distribution (Fig. 3B) was extracted from 3 to 32 Hz using a Morlet Wavelet. This started with 3 cycles and increased with a 0.1 factor. We considered the low-sigma (10–13 Hz) band, high-sigma (13–16 Hz) band, and the observed clear modulation within the high-beta (25–30 Hz) frequency band. For each band, the mean ERSP was computed within the Frontal and Central ROIs, while considering the temporal evolution over the whole epoch time course (Fig. 1A). Subsequently, we evaluated the ERSP within 1 s time-windows from sleep onset to 4 s after, considering the ERSP mean for each time-window (see Fig. 1B).

2.7. Quantification and statistical analysis

Statistical analyses were carried out in the R environment (R Core Team, 2021). Linear mixed models were fitted using the *lmer* function of the *lme4* package (Bates et al., 2015). The predictors were evaluated using Type III Wald $\chi 2$ tests, as implemented in the *Anova* function of the car package. We adopted linear mixed models with random intercepts per subject because we can assume that extracting features from the ERSP distribution or the spectrum of the same subject violated the assumption of independent observations due to individual variability. Therefore, we chose this model because it was a compromise that at least partially accounts for subject specificities while also avoiding the overfitting potentially given by setting random slopes due to the number of subjects involved in the study.

2.7.1. Sleep macrostructure

For the sleep macrostructure, the effects of the groups (S and BSI) and age-bin ((0–3)Y, Young and (3–6)Y, Old) were evaluated on the sleep statistics and spectrogram activities in the sigma and delta bands. For the sleep statistics, we considered the total sleep time (TST) in minutes and the percentage of stage 1 (N1), stage 2 (N2), and stage 3 (N3) NREM and stage REM on TST. TST is defined as the duration of time spent in Stages 1, 2, 3, and REM – the elapsed time from the onset of sleep through the last epoch of unambiguous sleep. NREM is defined as the duration of time in Stages 1, 2, and 3. A linear model was fitted using the *lm* function; it considered each sleep statistic independently as the dependent variable, while group and age-bin served as the predictors. The predictors were evaluated using an F test implemented in the *Anova* function of the *car* package (Fox and Weisberg, 2018). Because only a small percentage of participants reached the REM stage, this data was excluded from the subsequent analysis. The delta (0.5–4.75 Hz) and sigma (10–16 Hz) activities were extracted from the spectrogram, normalized to the mean band activity over all NREM sleep stages, and then averaged separately for N1, N2, and N3. Linear mixed models were fitted for each independent band. The mean power was taken as the dependent variable, while group, age-bin, and sleep stage (N1, N2, N3) served as the predictors. For both the sleep statistics and the sigma/delta activity analysis, the contrasts were further investigated with the *emmeans* function of the *emmeans* package (Lenth, 2022) by obtaining their estimated marginal means (EMMs). The effects were considered significant when $P < 0.05$ after the Bonferroni correction.

2.7.2. Sleep microstructure: spindle characteristics

In the first analysis, to provide an overview of the modulation of the spindle frequency distribution, the mean spindle frequency (SF) was evaluated by fitting a linear mixed model using the *lmer* function. SF was considered as the dependent variable, with group and age-bin serving as the between-subject factors, while the ROI was the within-subject factor. In the second analysis, we investigated the characteristics of slow and fast spindles on the Frontal and Central ROIs separately. We evaluated this by fitting a linear mixed model using the *lmer* function. The spindle density (#/min) and duration (s) were considered as the dependent variables, while the group, age-bin, and frequency band (10–13 Hz, Slow or 13–16 Hz, Fast) were evaluated in the LMM. In both analyses,
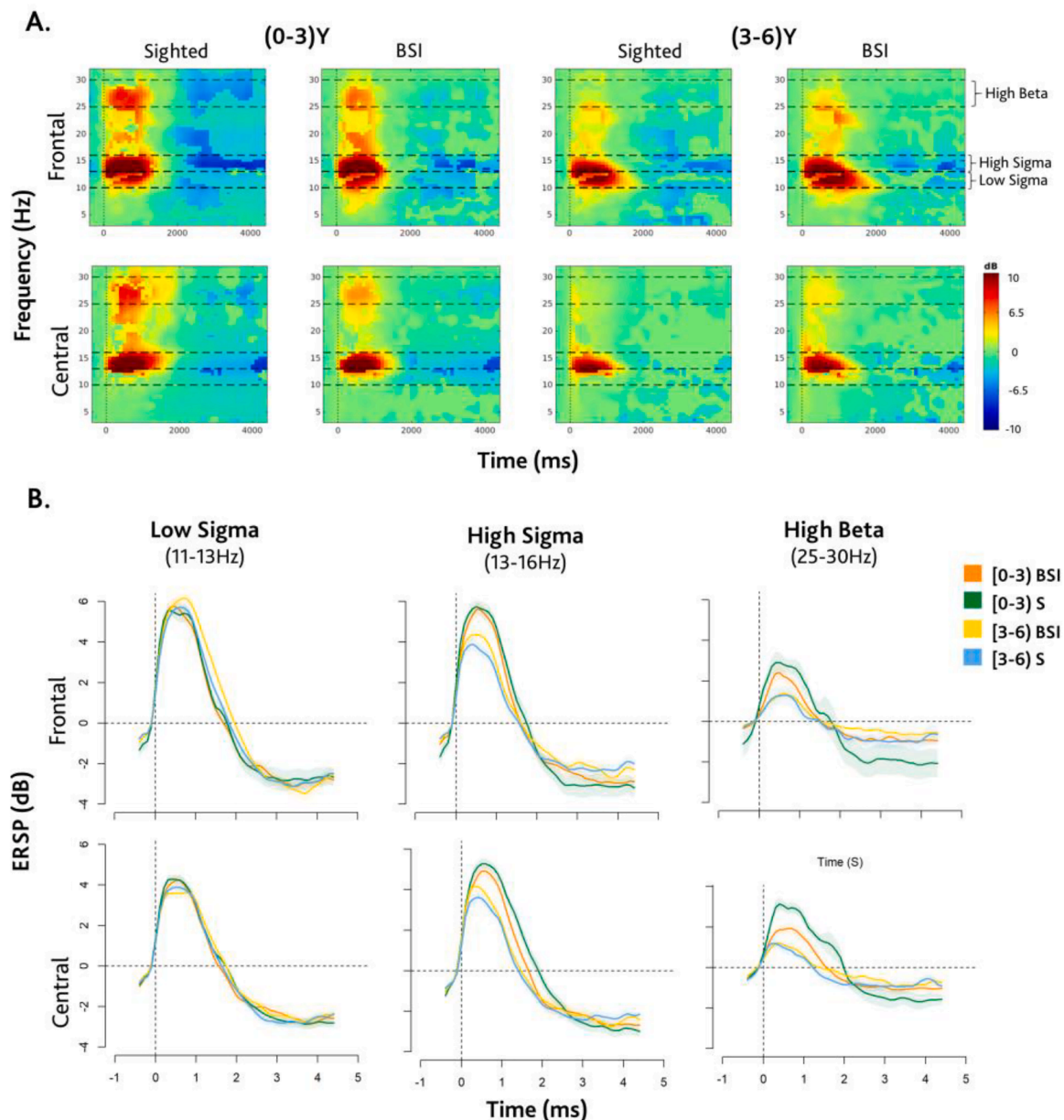
Fig. 1. Differences between age-bin, group, and ROI in ERSP power of sleep spindles. (**A**) Plot of time-frequency distribution for each group, age-bin, and ROIs showing the increase in low-sigma (10–13 Hz), high-sigma (13–16 Hz), and high-beta (25–30 Hz) power delimited by the horizontal dashed lines. We extracted event-related spectral perturbation (ERSP) in dB Hz using a Morlet Wavelet. Data were segmented from -1 s before the spindle onset to 4 s after it; the period from -1 to 0 s before the onset was used as the baseline. We computed the mean ERSP within each frequency band and ROI. Significant results were found for the high-sigma and high-beta. (**B**) ERSP curve representation of the low-sigma, high-sigma, and high-beta on the Frontal and Central ROIs for each group and age-bin. We considered ERSP peak within each frequency band on Frontal and Central ROIs. Significant results were found for the high-sigma and the high-beta only on the Central ROI.

the contrasts were further investigated using the *emmeans* function by obtaining the estimated marginal means (EMMs). The effects were considered significant when $P < 0.05$ after the Bonferroni correction. To evaluate the maturational effects in more detail, the analyses on spindle density and mean frequency were repeated while considering continuous age. Indeed, it is always suboptimal to dichotomize continuous variables. Thus, the planned contrasts were investigated with the *emtrends* function while considering age as a continuous covariate. Importantly, the figures that show these analyses have been generated using the *emmip* function of R, which creates an interaction plot of EMMs based on how they are fitted. Therefore, we have not aggregated the ages for statistical analysis. Rather, we have estimated the coefficients of the model and the associated 95 % confidence intervals. Then, we simulated

the prediction of the model and related a 95 % confidence interval at given ages. Thus, there is no quantization but only a graphic representation of the prediction of the model.

2.7.3. Sleep microstructure: spindle ERSP

The ERSP modulations were evaluated by fitting a linear mixed model using the *lmer* function. We considered the ERSP mean as the dependent variable, while the group, age-bin, and time-window ([0–1]s, [1–2]s, [2–3]s, [3–4]s) were evaluated in the LMM. The contrasts were further investigated using the *emmeans* function. The effects were considered significant when $P < 0.05$ after the Bonferroni correction. Afterward, to consider the interindividual variability, we also investigated the peak power within the spindle time-window ([0–2]s) for the

low-sigma (10–13 Hz), high-sigma (13–16 Hz), and high-beta (25–30 Hz) frequency bands and on both the Frontal and Central ROIs. In turn, we used the *aov* function to assess the effect of group and age-bin on peak power. The contrasts were further investigated with the *emmeans* function. We considered the comparisons to be significant when $P <$ 0.05 after the Bonferroni correction. To investigate the maturational effects in more detail, the analyses were repeated with continuous age instead of age-bins. Planned contrasts were investigated with the *emtrends* function while considering age as a covariate (see Section 2.6.2).

2.7.4. Association with clinical indices

Finally, we examined whether there was a specific association between the electrophysiological features and the selected clinical indices. First, we evaluated if the severity of visual impairment (i.e., Sighted (S) =0, Severely Visually Impaired (SVI) =1, and Blind (B) =2) could be predicted from the investigated spindle measures. To this end, we applied ordinal regression models using the *orm* function of the *rms* package. Subsequently, in the BSI children only, we related the spindle biomarkers with the specific clinical scores that reflect sensory, environmental interaction and motor dysfunction: the presence (or absence) of motor coordination impairment (MCI) and hypotonia (evaluated through neurologic examinations), along with the subsequent subscales of the RZS (Reynell, 1978): social adaptation (concerning personal autonomies), spatial exploration (i.e., the ability of the toddler to orient within a space), verbal comprehension (including the response to sound), and expressive language, to evaluate the social interaction. All the parameters were coded with Normal=1 or Altered=2. These data were not available for 5 participants. Then, to identify more reliable factors, we performed a factorial analysis in which we included all these indices (Drasgow, 2004; Revelle, 2009). This factorial analysis was based on a polychoric correlation matrix (Presaghi and Desimoni, 2023; Revelle, 2016). Parallel analysis suggested that 2 clinical factors were most appropriate. The first clinical factor was *environmental interaction*, which accounted for spatial exploration, sound response, social adaptation, and language indices. The second clinical factor was *motor disorders*, which accounted for motor coordination impairment and the hypotonia indices. For each clinical factor, we computed related scores. Then, we used the two extracted factors, instead of the original 6 indices, to test their possible associations with electrophysiological features.

To test the association between spindle biomarkers and clinical factors, we applied linear regression models. For each clinical factor in the first model, we considered the age-bin, while in the second model, we considered continuous age.

3. Results

To investigate our hypothesis that fast spindle development may be specifically affected in blind children, we recorded nap video-EEG in 50 blind or severely visually impaired (BSI) children and 64 sighted (S) children aged 5 months to 6 years old. We explored both macro- and micro-structural aspects. The macrostructural analyses provided information about sleep statistics (TST and %N1, N2, N3, NREM, and REM) and the activity of the sigma (10–16 Hz) and delta (0.5–4.75 Hz) bands at the different stages. No relevant differences were found between the BSI and S children (see supplemental information and Table S2). In the microstructural analyses, we focused on three potential spindle biomarkers: spatial spindle-frequency distribution on the scalp, spindles characteristics (both density and duration), and spindles' event-related spectral perturbation (ERSP) after the spindle onset in the different ROIs. Finally, we investigated the possible associations between spindle biomarkers and the indices of perceptual, environmental interaction, and motor impairment in BSI children.

3.1. The impact of blindness is ascribed to the central ROI

To ascertain an overview of the spindle topography distribution, we investigated the mean spindle frequency (SF). This measure allowed us to explore how the spindle frequency is distributed in different regions. Therefore, we fitted an LMM to evaluate the effects of group (S or BSI), age-bin (Young or Old), and ROIs (Central or Frontal) on SF. For SF, a significant interaction occurred between group, age-bin, and ROI, $\chi2$ (1)=99.89, $P < 0.0001$. Fast spindles were localized mainly in the central area while slow spindles were localized mainly in the frontal area (see Fig. 2B). Indeed, the SF was higher in the central than the frontal ROI in all groups and age-bins: young S, $Z = 11.21$, $P < 0.0001$, young BSI, $Z = 13.94$, $P < 0.0001$, old S, $Z = 27.24$, $P < 0.0001$, and old BSI group, $Z = 22.74$, $P < 0.0001$. Furthermore, as they aged, S children had the typical reduction both on the frontal, $Z=-5.03$, $P < 0.0001$, and central, $Z=-3.07$, $P = 0,03$, ROIs; in contrast, this reduction was not evident in the BSI children. Considering continuous age, the analysis provided evidence of a selective absence of SF maturation on the central ROI in BSI children (see Fig. 2C). Indeed, the results showed the typical reduction with age in both the frontal and central ROIs in S children, $Z=-4.6$, $P < 0.0001$ and $Z=-3.09$, $P = 0.002$, respectively; and only in the frontal region, $Z=-3.50$, $P = 0.0005$, in the BSI group. The between-group contrasts provided evidence of a significant interaction in the central area, $Z = 2.08$, $P = 0.04$.

3.2. Maturational differences in spindle characteristics

During development, changes in the characteristics of the slow and fast spindles reflect the maturation of the thalamocortical structures (D'Atri et al., 2018; Guadagni et al., 2021; Ricci et al., 2021; Scholle et al., 2007). Therefore, we investigated spindle characteristics by fitting an LMM to evaluate the effects of group (BSI or S), age-bin (Young and Old), and frequency band (Slow or Fast) on the spindles' density (#/min) and duration (s) on each of the frontal and central ROIs separately. The BSI children diverged from their S peers in the maturation of slow and fast spindles length and density only in the central area, $\chi2(1)=$ 125, $P < 0.0001$ and $\chi2(1)=11.60$, $P = 0.0003$. Specifically, in S children, the fast spindles were longer than the slow spindles for the young age-bin, $Z = 19.34$, $P < 0.0001$, while the slow spindles were longer than the fast spindles for the old age-bin, $Z=-8.10$, $P < 0.0001$. Indeed, there is a reduction of the fast spindles duration between age-bins, $Z=-3.3=$, $P = 0.01$ (Fig. 3A). This result was confirmed by continuous-age analysis, $Z=-4.62$, $P < 0.0001$. In the BSI children, the fast spindles were longer in the young age-bin, $Z = 6.04$, $P < 0.0001$, without any changes with age. The continuous-age analysis only revealed a slight reduction of the fast spindles' duration with age, $Z=-2.20$, $P = 0.03$ (Fig. 3C). Concerning spindle density, the fast spindles were denser than the slow spindles in young S children, $t(106) =5.4$, $P < 0.0001$, while there was no density difference in the young BSI children. Moreover, between age-bins, we found a maturation of both the slow and fast spindles only in the S children. Specifically, the fast spindles were denser in the young age-bin, $t(212)=-3.1$, $P = 0.02$, while the slow spindles were denser in the old age-bin, $t(212)=3.8$, $P = 0.003$ (Fig. 3B). The continuous-age analysis confirmed that only in the S children, the fast spindles' density decreased with age, $t(220)=-3.47$, $P = 0.0006$, while the slow spindles' density increased with age, $t(220)=4.12$, $P = 0.0001$ (Fig. 3D). Indeed, the contrasts between the BSI and S children prove a significant divergence in the maturation of both the slow, $t(220)=-3.34$, $P = 0.001$, and fast spindles, $t(220)=2.20$, $P = 0.03$.

3.3. High-sigma and high-beta in spindles ERSP

Another important spindle measurement is an event-related spectral perturbation, especially when splitting whole sigma activity into low- and high-sigma, which are respectively associated with slow and fast spindles. Considering ERSP went beyond the global spindle descriptors,
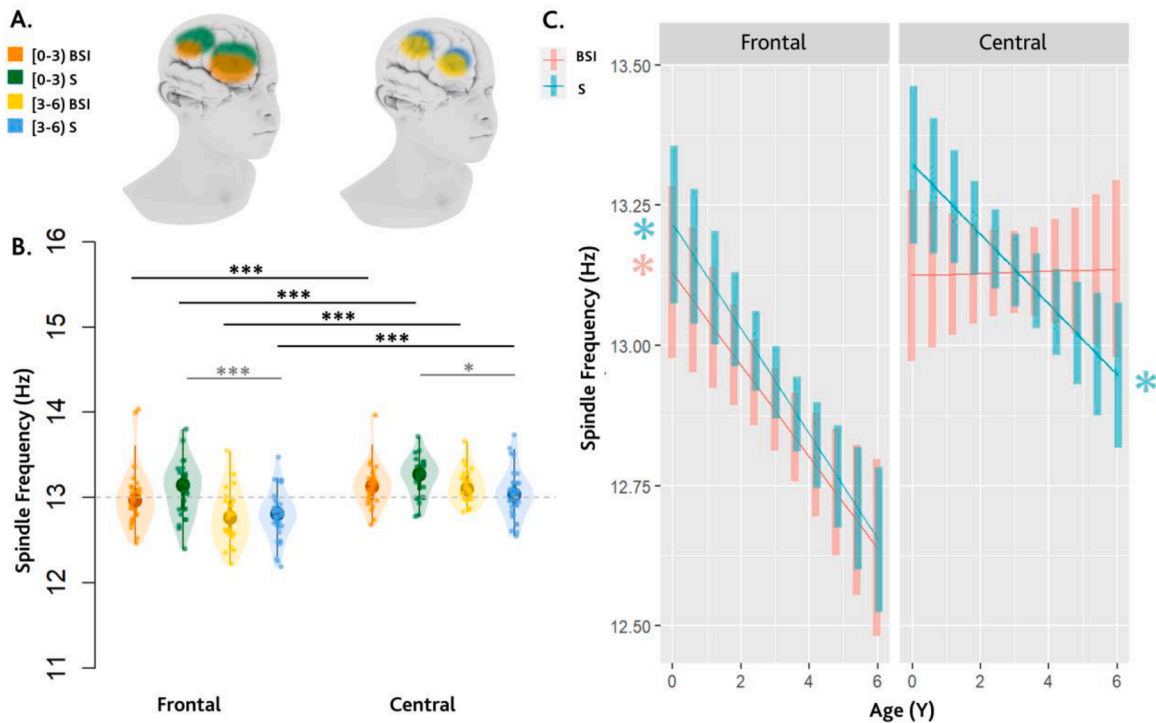
Fig. 2. Topographical distribution of mean spindle frequency (SF) comparing the Frontal and Central ROIs. (A) The 3D models represent the group differences between the two age-bins ((0,3)Y 270 and (3,6)Y) and the different ROIs (Frontal and Central). The main difference is related to the central spindles' power in the early age-bin, which is weaker in blind (orange) children than in sighted (green) children. In the older age-bin, the spindle power decreases in sighted children (light blue), while it remains weak in blind children (yellow). **(B)** Plot of mean spindles frequency (violin plot), the median (box plot) and related 95 % CI (vertical line), and the single subjects spindle frequency (scattered plot) for each age-bin, group, and ROIs. The dashed line points out $y = 13$. The stars represent the significant p values (* = $p < 0.5$, **=$p < 0.01$, ***=$p < 0.001$) after the Bonferroni correction considering the significant interaction. The gray stars represent the significant interactions within the ROIs (effects of group and age-bin); the black stars represent the significant interactions between the ROIs (differences in frontal and central area). (**C**) Plot of the frontal and central spindle frequency evolution considering age as a continue variable. The blue stars represent the significant evolution of sighted participants, while the pink star of the BSI children. The bigger stars represent a significant p value < 0.001.

and it explored the frequency distribution and the timing of the activation of each frequency during the spindle event. Some studies reported a concurrent high-frequency activity with spindles in animals (Averkin et al., 2016) and humans (Clemens et al., 2011). Only one study presented evidence of a concurrent component time-locked to the spindle, spanning from ~ 24 to 30 Hz, in the centro-parietal areas (Laventure et al., 2018). Accordingly, a first visual inspection of the spindle ERSP sometimes provides evidence of an increased occurrence of high-beta power (Fig. 1A). Therefore, we decided to also explore this frequency band.

For each ROI, we fitted an LMM to evaluate the effects of age-bin and group on the mean ERSP in 1-s time windows from 0 to 4 s after the spindle onset. Differences between age-bins and groups emerged in the high-sigma and the high-beta on the Central ROI (see Table 1, Fig. 4A, and Fig. 4B). Within the high-sigma band, the Y S children showed higher activity than their BSI peers in the second time window. However, in the continuous age analysis, the difference was found in both the [0–1]s and [1–2]s time windows. Moreover, the power was strikingly higher in the Y S children than the O S children in both the first and second time windows. This maturational difference was almost absent in the BSI children, with a weak significant difference only in the [0–1]s time window. As shown in Fig. 4B, these maturational results were confirmed by the continuous age analysis, which showed evidence that a 3- to 4-year period is crucial for the differences in spindle development to occur between BSI and S children. Similarly, the high-beta band power was higher in Y S children than in BSI children in the first two time windows. This effect of the group also persisted when considering continuous age. Moreover, the high-beta activity is higher in Y S children than in O S children. In turn, no developmental differences were

found in the BSI children. By evaluating continuous age, we confirmed these results (see Fig. 4B).

To consider interindividual variability, we also investigated the effects of group and age on peak power in the spindle time window ([0–2] s). We found similar results in the age-bin and continuous age analysis (see Table 2, Figs. 4C and 4D). Differences involved the central ROI in the high-sigma band and the high-beta band, with a maturational evolution only occurring in S children. The high-beta band also showed that peak power is higher in Y S children than in BSI children. However, a significant interaction between BSI and S children was found on both high-sigma and high-beta when considering age as a continuous variable.

3.4. Sleep spindles and their association with clinical factors

Recent studies have demonstrated that fast spindles could be an important developmental biomarker in infancy (Jaramillo et al., 2023). Therefore, we hypothesized that the deviation from the typical developmental trajectory of fast spindles in blind children could be linked to possible sensorimotor disorders. Thus, we tested the association between our spindle biomarkers and specific clinical indices in BSI children. For the visual impairment index (VII), our results showed evidence that sleep density and spindle ERSP were good predictors. Specifically, we found a significant interaction between age-bin, spindle frequency band, and density, $\chi^2(1) =12.39$, $p = 0.0004$. Comparable results were found in the continuous age model, $\chi^2(1) =12.02$, $p = 0.0005$. Fig. 5A shows that the lower the fast spindle density is in the (0–3)Y age-bin, the higher the probability that they will be blind subjects. In turn, the higher the fast spindle density is in the (3–6)Y age-bin, the higher the
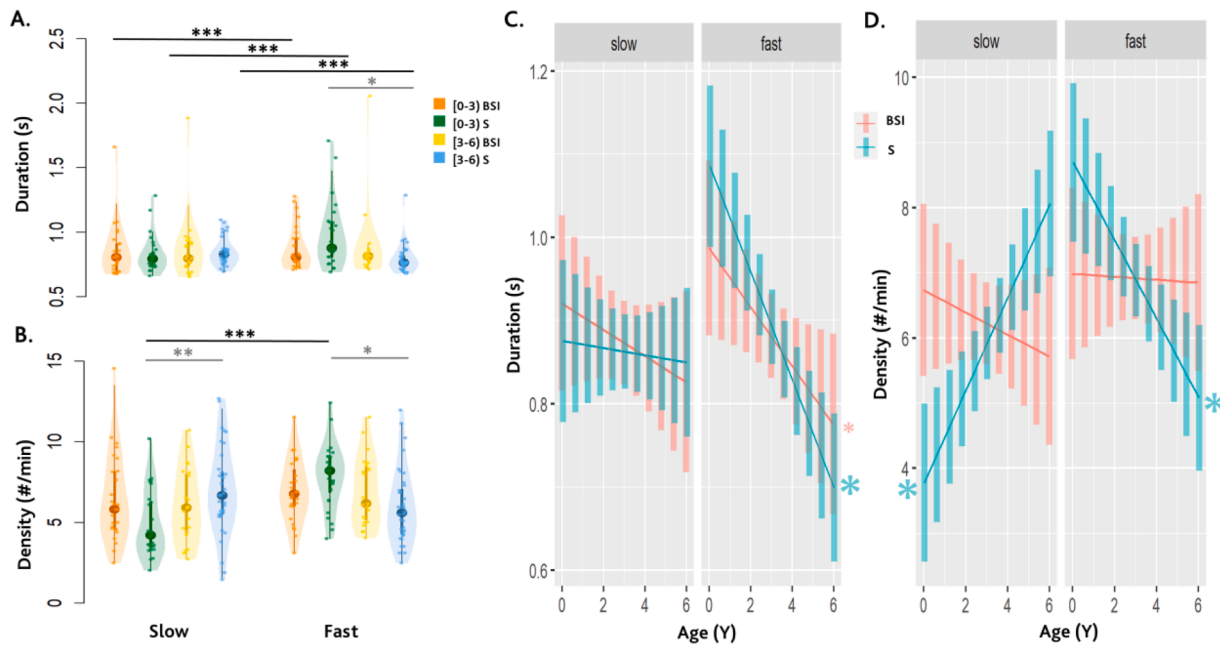
Fig. 3. Differences between age-bin and group in duration and density of fast and slow spindles. (**A**) Plot of mean spindles duration (violin plot), the median (box plot) and related 95 % CI (vertical line), and the single subjects spindle duration (scattered plot) for each age-bin, group, and frequency band. (**B**) Plot of mean spindles density (violin plot), the median (box plot) and related 95 % CI (vertical line), and the single subjects spindle density (scattered plot) for each age-bin, group, and frequency band. In both figures A and B, the stars represent the significant P values (*=$p < 0.5$, **= $p < 0.01$, ***= $p < 0.001$) after the Bonferroni correction. The gray stars represent the significant interactions within the spindle frequency band (effects of group and age-bin); the black stars represent the significant interactions between the spindle frequency band (differences in slow and fast spindles). (**C**) Plot of the slow and fast-spindles evolution of duration considering age as a continue variable. (**D**) Plot of the slow and fast spindle density evolution considering age as a continue variable. In both figures C and D, the blue stars represent the significant evolution of sighted participants, while the pink star of the BSI children. The bigger stars represent a significant P value < 0.001; the small star represents a significant P value < 0.05.

Table 1

Statistics of mean spindle ERSP. The table shows the statistics of the LMM which evaluate effects of age-bin and group (BSI = blind/severely visually impaired, S=sighted) on mean ERSP only on Central ROI. Models are expressed with the Wilkinson notation.

		Low Sigma				High Sigma			High Beta			
Mean ERSP Age-bin *Mean frequency ~ time window*group*age bin + (1|subject)*												
		χ^2(Df)	p			χ^2(Df)		p	χ^2(Df)		p	
time_window*group*age_bin		1.46(3)	0.69			9.36(3)		0.02	11.66(3)		0.009	
Post Hoc for each time window												
		[0–1] s		[1–2] s		[0–1] s		[1–2] s		[0–1] s		[1–2] s
		t (Df)	p	t (Df)	p	t(Df)	p	t(Df)	p	t(Df)	p	t(Df)	p
BSI-S contrast	(0–3) Y	–	–	–	–	–	–	−2.87 (377)	0.004	−1.98 (392)	0.048	−2.92	0.004
BSI-S contrast	(3–6) Y	–	–	–	–	–	–	–	–	–	–	–	–
(0–3)Y − (3–6)Y contrast	BSI	–	–	–	–	–	–	2(377)	0.046	–	–	–	–
(0–3)Y − (3–6)Y contrast	S	–	–	–	–	3.62 (377)	0.0003	5.13 (377)	<0.0001	3.59 (392)	0.0004	3.75 (392)	0.0002
Mean ERSP Age *Mean frequency ~ time window*group*age bin + (1|subject)*												
		χ^2(df)	p			χ^2(df)		p	χ^2(df)		p	
time_window*group*age		2.17(3)	0.5			9.09(3)		0.03	14.31(3)		0.002	
Post Hoc for each time window												
		[0–1] s		[1–2] s		[0–1] s		[1–2] s		[0–1] s		[1–2] s
		t (Df)	p	t (Df)	p	t(Df)	p	t(Df)	p	t(Sf)	p	t(Df)	p
BSI-S contrast		–	–	–	–	2.04 (384)	0.04	2.59 (384)	0.01	1.91 (393)	0.056	2.21 (393)	0.03
BSI		–	–	–	–	–	–	−2.17 (384)	0.03	−2.07 (393)	0.04	–	–
S		–	–	–	–	−4.64 (384)	<0.0001	−6.46 (384)	<0.0001	−5.31 (393)	<0.0001	−4.66 (393)	< 0.0001

probability that they are blind subjects. In contrast, the slow spindles have the opposite pattern. The SVI group seems to follow the S group at low densities, and the B group at high densities for fast spindles in the

0–3 years (note: this occurs in the opposite way for the slow spindles). In contrast, in the (3–6)Y age-bin, they have a pattern similar to the B group.
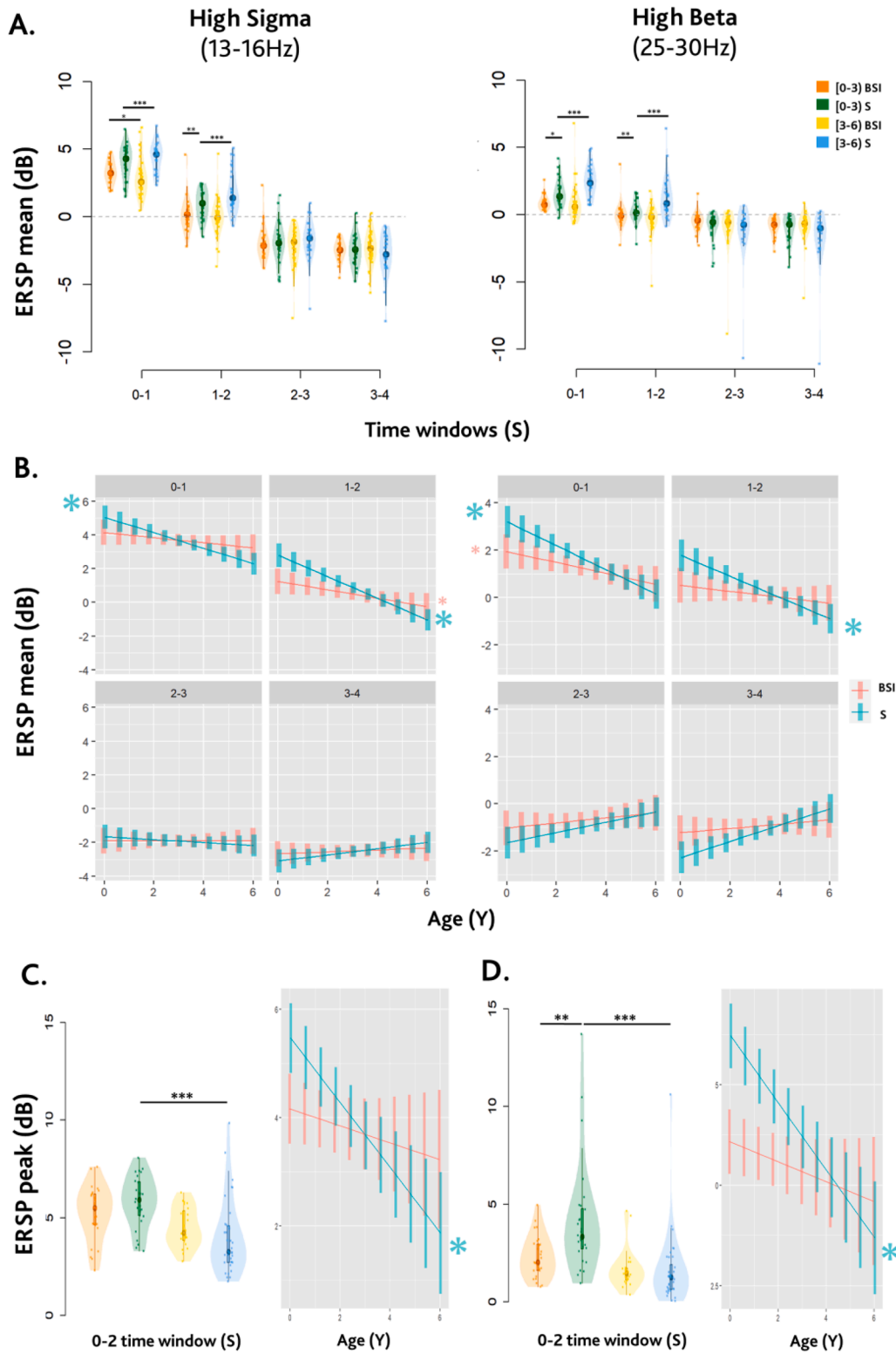
(caption on next page)

Moreover, we found a significant interaction between age-bin and mean ERSP in the high-sigma band, $\chi^2(2) =10.51$, $p = 0.005$, and high-beta band, $\chi^2(2) =10.31$, $p = 0.006$. These interactions persisted when considering age as a continuous variable, showing results of $\chi^2(2)=11.59$, $p = 0.003$ and $\chi^2(2)=8.44$, $p = 0.01$, respectively. Similarly, we found a significant interaction between age-bin and peak ERSP in the high-sigma band, $\chi^2(1) =6.99$, $p = 0.008$, and high-beta band, $\chi^2(1) =4.8$, $p = 0.03$. Once again, these interactions were confirmed when considering age as a continuous variable, showing results of $\chi^2(1)=9.91$, $p = 0.002$ and $\chi^2(1)=5.17$, $p = 0.02$, respectively. The probability curves are shown in Figs. 5B and C for ERSP mean and peak, respectively. They reveal similar results. Specifically, the lower the high-sigma and high-

Fig. 4. Mean and peak ERSP within high-sigma (13–16 Hz), and high-beta (25–30 Hz) on Central ROI. Plots A and B represent the Mean ERSP, plot C and D represents the Peak ERSP. **(A)** Plot of Mean ERSP within high-sigma and high-beta on the Central ROI within 1 s time windows from the spindle onset through 4 s after (violin plot), the median (box plot) and related 95 % CI (vertical line), and the single subjects Mean ERSP (smaller points). The dashed line points out $y = 0$. The stars represent the significant P values (*=$p < 0.5$, **= $p < 0.01$, ***= $p < 0.001$) after the Bonferroni correction. Stars represent the significant interactions within groups (effects of age-bin) and between groups (differences between the BSI and S groups). **(B)** Plot of the Mean ERSP evolution in each time window considering age as a continue variable. The blue stars represent the significant evolution of S participants, while the pink star of the BSI children. The bigger stars represent a significant p value < 0.001; the small star represents a significant P value < 0.05. **(C)** and **(D)** represent the Peak ERSP within high-sigma and high-beta, respectively, on Central ROI. On the left, plot of Peak ERSP in the spindle time window [0–2]s (violin plot), the median (box plot) and related 95 % CI (vertical line), and the single subjects Mean ERSP (smaller points). The stars represent the significant P values (*=$p < 0.5$, **= $p < 0.01$, ***= $p < 0.001$) after the Bonferroni correction. On the right, plot of the Peak ERSP evolution in the spindle time window [0–2]s considering continuous age. The bigger blue star represents the significant evolution of sighted participants with significant P value < 0.001.

Table 2
Statistics of peak spindle ERSP. The table shows the statistics of the LMM which evaluate effects of age-bin and group (BSI = blind/severely visually impaired, S=sighted) on mean ERSP only on Central ROI.

		Low Sigma		High Sigma		High Beta	
Peak ERSP Age-bin *Peak frequency ~ group*age bin*							
		F(Dfn, Dfd)	**p**	**F(Dfn, Dfd)**	**p**	**F(Dfn, Dfd)**	**p**
*Group*age bin*		0.03(1110)	0.87	4.02 (1110)	0.047	7.1(1110)	0.0087
Post Hoc							
		t(Df)	**p**	**t(Df)**	**p**	**t(Df)**	**p**
BSI-S contrasts	(0–3)Y	–	–	–	–	3.65(110)	0.0016
BSI-S contrasts	(3–6)Y	–	–	–	–	–	–
(0–3)Y – (3–6)Y contrasts	BSI	–	–	–	–	–	–
(0–3)Y – (3–6)Y contrasts	S	–	–	−5.06(110)	<0.0001	−5.45(110)	<0.0001
Peak ERSP Age *Peak frequency ~ group*age + Error(subject)*							
		F(Dfn, Dfd)	**p**	**F(Dfn, Dfd)**	**p**	**F(Dfn, Dfd)**	**p**
*Group*age*		2.17(1110)	0.87	6.66(1110)	0.011	7.57(1110)	0.0069
Post Hoc							
		t(Df)	**p**	**t(Df)**	**p**	**t(Df)**	**p**
BSI-S contrast		–	–	2.58(110)	0.011	2.75(110)	0.0069
BSI		–	–	–	–	–	–
S		–	–	−5–32(110)	<0.0001	−5.95(110)	<0.0001

beta power were in the (0–3)Y age-bin, the higher the probability that they were classified as blind subjects. In the (3–6)Y age-bin, a higher high-sigma increases the probability of visual disorder. The SVI group showed a similar behavior as for fast spindle density.

Regarding the clinical factors *environmental interaction* and *motor disorders*, a trend emerged for the interactions between age-bin, time window, and ERSP mean in the high-sigma band for the *motor disorders*, F(1,78) =3.7, $p = 0.057$. However, this interaction was fully significant when considering continuous age, showing results of F(1,78) =5.7, $p = 0.02$. Specifically (see Fig. 5D), for (3–6)Y children within the [0–1]s time window, a higher high-sigma activity increased the score of the *motor disorders* factor. Finally (see Fig. 5D), we found a main effect of a high-beta ERSP peak for the *motor disorders* factor, F(1,39)=4.89, $p = 0.03$, which shows a negative association.

4. Discussion

Spindles are a marker of sensory information reprocessing and consolidation during sleep (Fernandez and Lüthi, 2020; Fogel and Smith, 2011; Gruber and Wise, 2016). In turn, how their characteristics change may be a marker of optimal or deviant neurodevelopment. We hypothesized that blindness may elicit a plastic reorganization of the brain structures that are involved in spindle generation and that this would specifically affect the development of fast spindles. Indeed, fast spindles are specifically associated with sensorimotor processing (Barakat et al., 2011; Chatburn et al., 2013; Jaramillo et al., 2023; Schabus et al., 2007; Tamaki et al., 2008), which is often compromised by visual deprivation. We focused on three spindle biomarkers that had notable differences between BSI and S children. First, we found an absence of

mean frequency reduction only on the central ROI in the BSI children. This suggests a selective involvement of the sensorimotor area. Second, the BSI children did not show maturation (or showed just a slight maturation) of the fast spindles' density and duration. Third, the ERSP mean and peak provided evidence of the specific impact that blindness had on the high-sigma and high-beta in the central ROI. Finally, in the BSI children, we found associations between spindle biomarkers and the indices of perceptual, and motor impairment.

4.1. The impact of blindness is ascribed to the central area

The topography of spindles is modulated by experience-dependent plasticity (Menicucci et al., 2022; Tononi and Cirelli, 2014). Therefore, we hypothesized that congenital blindness could impact the maturation of spindles in the area linked to the processing of sensorimotor information. Accordingly, our results provided evidence of an absence of mean frequency reduction only on the central ROI in blind and severely visually impaired (BSI) children. As shown in our results and in the literature, a decrease in mean frequency in both the frontal and central ROI is typically present in children between ages 2 to 5 years (D'Atri et al., 2018; Kwon et al., 2023; McClain et al., 2016). Indeed, these changes reflect the typical neural development that occurs from infancy to adolescence, and it includes synaptic pruning. It consists of removing the weaker synaptic connections so that they produce fewer but more efficient synapses (Rapoport et al., 2001). Therefore, the lower the mean spindle frequency is, the lower the activity necessary to obtain the same results; this reflects an efficient process. However, in BSI children, the lack of vision from birth seems to influence the related brain structures, which is reflected in this process being less optimized.
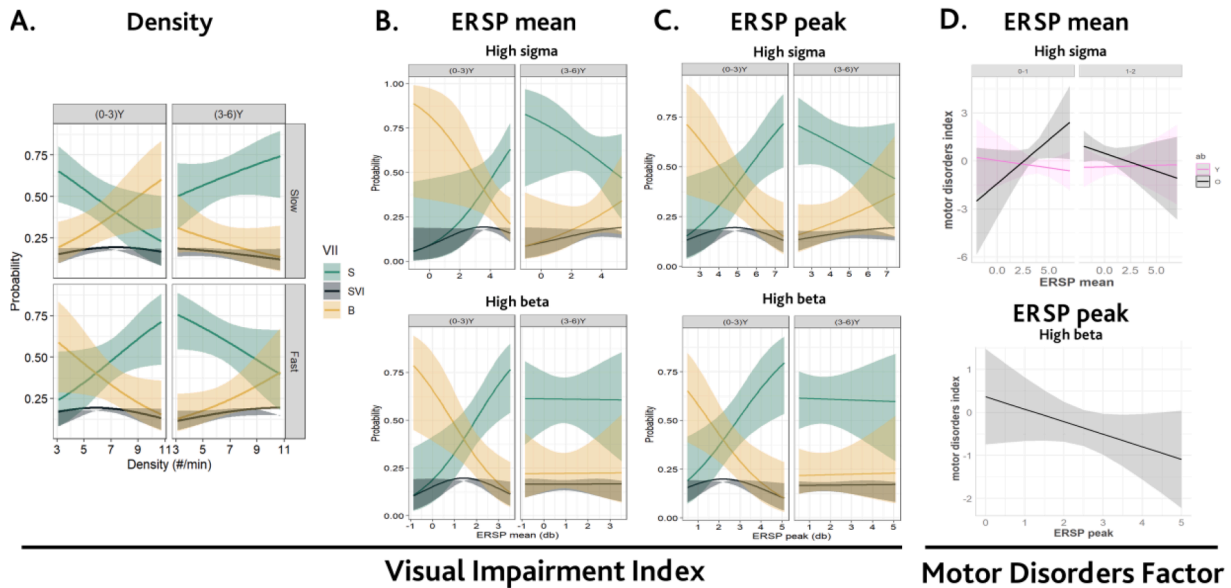
Fig. 5. Spindle biomarkers association with clinical indices. figures (**A**), (**B**) and (**C**), show the results of Visual Impairment index (VII). Specifically, they are the plot of probability to be classified as S, SVI and B based on slow and fast spindle density (**A**), based on high-sigma and high-beta ERSP mean (**B**), and high-sigma and high-beta ERSP peak (**C**). figures (**D**) show the results of motor disorders factor, and specifically the association with spindle ERSP in the high-sigma (top) and high-beta (bottom) bands.

The topography of spindles also partially reflects the slow and fast spindles subdivision because slow spindles prevail in the frontal area, while fast spindles in the central one (Chatburn et al., 2013; D'Atri et al., 2018). As expected, our results showed that the spindle frequency is higher in the central area than in the frontal area, confirming the typical topography spindle distribution. This finding suggests that the impact on the central area by blindness could mirror a possible maturational divergence of fast spindles.

A compromise of high-frequency spindles' mechanisms could also explain why the spindle frequency of the BSI children seems to start slower. We can speculate that BSI children had slower spindle frequency in their early lives may be related to processes occurring in their first six months of life, which are not considered in the current study. Some studies have revealed that in the first months of life, there is an increase in spindle frequency and that decreases occur only later (D'Atri et al., 2018; Kwon et al., 2023; Louis et al., 1992). Even though we still cannot clearly distinguish fast from slow spindles at this age (more studies should be done to determine this), it is clear that the mechanisms that favor the maturation of high frequencies accelerate at this stage. This is probably due to an increase in the synaptic connections related to the processing of sensory and motor information. Therefore, a possible interpretation is that these mechanisms are already corrupted in blind children. Consequently, they show a lower level of spindle frequency in the first years of life than sighted children do. Generally, spindle frequency may indicate network maturity (Kwon et al., 2023), which suggests that blindness could impact the cortical maturation of our early lives.

4.2. Developmental differences of fast spindles

Sleep spindles are the first EEG hallmarks to mature after birth (Eisermann et al., 2013; MacLean et al., 2015; Sankupellay et al., 2011; Scholle et al., 2007). Thus, changes in their characteristics reflect the maturation of the thalamocortical network (D'Atri et al., 2018; Guadagni et al., 2021; Ricci et al., 2021; Scholle et al., 2007). After exploring the spindle frequency distribution on the scalp, we investigated the slow and fast spindles' density and duration in frontal and central areas separately. We found that the spindles' density and duration were different only in the central area where the BSI children did not show (or just slightly show) the maturation of fast spindles.

Fast spindles, which are linked to sensorimotor (Schabus et al., 2007) and neural processing (Geiger et al., 2011; Lustenberger et al., 2012; Maquet, 2010), undergo greater changes with age in this period of life. Indeed, their density is higher during infancy, and it significantly decreases with age. Changes in spindle duration follow a similar developmental trajectory, according to the literature (Kwon et al., 2023). As such, the absence of this spindle evolution in BSI children underlies the loss of those synaptic changes that should have occurred during the earliest stages of life, which allows the neural structures to mature correctly. Indeed, changes in spindle density and duration are linked with the trajectory of cortical growth (Kwon et al., 2023). Specifically in central regions, the cortical gray matter increases in the first year of life due to ongoing neural mechanisms, such as neurogenesis, synaptogenesis, and spine density formation (Bhardwaj et al., 2006; Sanai et al., 2011). Subsequently, the cortical thickness begins to decrease, which reflects synaptic pruning (Gilmore et al., 2018). Thus, spindle density and duration may reflect cortical replay and consolidation (Kwon et al., 2023).

Interestingly, we also found an absence of slow spindle maturation in the central area of BSI children. Although the evolution of slow and fast spindles that occurs with age may reflect the maturation of different subnetworks, our results suggest that the maturation of slow and fast spindles could be correlated. However, the current study is based on an arbitrary definition of the frequency range of slow and fast spindles rather than using a single-subject method for determining the frequency bands of the spindles based on the position of spectral peaks (Ujma et al., 2016). Future studies may benefit from a single-subject approach to identify subgroups of spindles and better elucidate the developmental dynamics of slow and fast spindles. Based on our results, we can suggest that blindness could have a pivotal impact on the neural processing and consolidation operated by the thalamocortical network that occurs in the first years of life (Piantoni et al., 2013; Steriade et al., 1985; Tarokh et al., 2014).

4.3. High frequencies spindles ERSP

The spindle ERSP allows us to go beyond global spindle descriptors, exploring the frequency, distribution, and activation timing during the spindle event. The ERSP mean and peak provided evidence of the

specific impact that blindness had on the high-sigma region in the central ROI. In the sighted children, we found a striking power reduction with age for both spindle time windows ([0–1]s, [1–2]s). In contrast, this maturational difference was just barely hinted at in the BSI children.

Our results indicate that the typical developmental trajectory of the fast spindles does not occur in BSI children, suggesting that vision is extremely important in the proper maturation of the neural structures that underlie brain rhythms. While this importance has already been demonstrated for awake cortical (i.e. alpha) (Campus et al., 2021) rhythms, our pioneering results extend it to sleep rhythms for the first time. It is well known that sleep promotes the stabilization of visual plasticity, which is revealed by temporary visual deprivation (Aton et al., 2013; Menicucci et al., 2022); however, researchers have not yet studied how the absence of vision from birth affects the development of the sleeping brain. The selective involvement of the high-sigma and central regions suggests that it has a strong link with processing sensorimotor information.

Interestingly, the spindle ERSP also revealed a high-beta synchronization with a pattern similar to that of high-sigma. Some studies reported a concurrent high-frequency activity with the spindles in animals (Averkin et al., 2016) and humans (Clemens et al., 2011). Only one study presented evidence of a concurrent component time-locked to the spindle, spanning from ∼ 24 to 30 Hz, in the centro-parietal areas (Laventure et al., 2018). The researchers described it as a secondary spindle component that represents the activity of a neuron's population synchronized with spindle oscillations. Specifically, the authors found that following a motor-learning task, a sensory cue provided during sleep improved performances and modulated high-beta activity during spindle oscillation. Another study found increased high-frequency activity over the motor cortex during NREM sleep (Nobili et al., 2011). This beta modulation may have been a reinforcement activity of reprocessing sensory and motor information. Mechanisms that could be affected in early blind infants favor the development of multisensory and motor impairments that can be found during development.

4.4. Sleep spindles and sensorimotor processing

Sleep spindles provide a direct window into thalamocortical maturation and insights into the development of the sensorimotor and cognitive functions that they support (Kwon et al., 2023). A recent study demonstrated that fast spindles could be an important developmental biomarker in infancy (Jaramillo et al., 2023). The researchers found that infants with higher fast-spindle density at 6 months old showed higher developmental scores at both 12 and 24 months, including their Gross Motor Scores. These findings validated the role fast spindles play in predicting sensorimotor scores. Behaviors that fall within the perceptual and motor realm are often compromised in blind children. A strong visual impairment from birth affects children's exploration of their own bodies and the external world (Rigato et al., 2014). This compromises their spatial representation development (Cappagli et al., 2019, 2017; Gori et al., 2021) and leads to increased difficulties in establishing social relationships with their peers (Cappagli et al., 2017; Houwen et al., 2007). These difficulties reduce interactions with reality, which may lead to the altered development of motor abilities (Cappagli et al., 2019; Houwen et al., 2007, 2009).

Therefore, we investigated if a deviation from the typical developmental trajectory of fast spindles in blind children could be linked to possible sensorimotor disorders. Our results provided evidence that sleep density and the spindle ERSP's mean and peak are good predictors of visual impairment. Specifically, a lower density of fast spindles in the younger group of children and a higher density in the older group of children were associated with a higher probability of having a visual impairment. Similarly, the probability of blindness increased with lower high-sigma and high-beta activity in the young age-bin, while there was only a higher activity of the high-sigma bands in the older children. These results support that blindness itself, not the disease or injury that

caused it, causes changes in the spindles. The SVI group seems to have a hybrid behavior in the first years of life, which becomes more like the blind group with age. The spindle ERSP mean in the high-sigma band may be also an interesting biomarker of motor disorders in the older group of BSI children. A high-sigma ERSP mean seems to represent the more important spindle measure; it can predict both visual impairment in early life and later motor dysfunction.

This temporal dynamic emerges from the analysis using the age-bins compared to the analysis that examines continuous age. In general, in the measures we considered, we found similar results between the two models. This suggests that three years of age may represent a meaningful threshold in measuring the developmental differences in the neurophysiological markers of sleep between blind and sighted children; this also holds in wakefulness. A possible explanation is that during the third year of age, there is an abrupt transition in the function of sleep. During early development, sleep predominantly promotes brain reorganization; in contrast, during late development, the neuronal repair function of sleep is more dominant (Cao et al., 2020). We found some important differences between the groups in the first three years of life. This suggests that the brain reorganization function of sleep could be more involved, and there is also an effect on future deficits. Unexpectedly, the ERSP peak in the high-beta band can predict the motor dysfunction index independently from age. This is probably because it is more sensitive to interindividual variability.

These findings suggest that fast spindles and their concurrent beta modulation could be an important biomarker in blind children. Although further longitudinal studies are needed, and the association with specific tasks needs to be determined, the delay in the maturation of the thalamocortical network may represent the earliest impacted neurophysiological mechanism that could cause future impairment. Thus, sleep spindles seem to represent an early biomarker of a possible impairment. Moreover, recent evidence has shown that spindles not only mirror the thalamocortical activity but that they also have an active role in the thalamocortical network maturation (Schoch et al., 2021; Sokoloff et al., 2021). Indeed, sleep spindles favor the synaptic plasticity that gates the required dendritic calcium shifts (Seibt et al., 2017). Therefore, it can be hypothesized that there is a reciprocal cause-and-effect relationship between the maturation of the spindles and our sensorimotor skills.

5. Conclusions

Our study shows the importance of investigating the sleeping brain to identify the early biomarkers of developmental divergence in blind children. Sleep mechanisms could be an unexplored way to understand how sensory deprivation produces a neural divergence from the typical developmental trajectory. This information has considerable therapeutic implications, both in terms of timing (i.e., when to start intervening) and new therapeutic possibilities (Vitali et al., 2022) (i.e., considering both wake and sleep as possible intervention periods).

Data and code availability statement

All EEG raw data are publicly available on the Zenodo repository at the following link: https://zenodo.org/uploads/10200985.

The processing and analysis pipeline were performing functions of tools that are publicly available (EEGLAB: https://sccn.ucsd.edu/eeglab/index.php, R: https://www.r-project.org).

CRediT authorship contribution statement

Helene Vitali: Writing – original draft, Software, Formal analysis, Data curation, Conceptualization. **Claudio Campus:** Writing – review & editing, Validation, Software, Methodology, Formal analysis, Data curation. **Sabrina Signorini:** Writing – review & editing, Validation, Supervision, Project administration. **Valentina De Giorgis:** Writing – review & editing, Validation, Supervision, Resources, Investigation. **Federica Morelli:** Writing – review & editing, Validation, Methodology, Investigation, Data curation. **Costanza Varesio:** Writing – review & editing, Validation, Investigation, Data curation. **Ludovica Pasca:** Writing – review & editing, Visualization, Validation, Investigation. **Alessia Sammartano:** Writing – review & editing, Validation, Investigation, Data curation. **Monica Gori:** Writing – review & editing, Visualization, Validation, Supervision, Resources, Project administration, Funding acquisition.

Declaration of competing interest

Authors declare no conflict of interest.

Data availability

The datasets generated from this study can be found in online Zenodo repository at the following link: https://zenodo.org/uploads/10,200,985.

Supplementary materials

Supplementary material associated with this article can be found, in the online version, at doi:10.1016/j.neuroimage.2024.120508.

References

Aton, S.J., Broussard, C., Dumoulin, M., Seibt, J., Watson, A., Coleman, T., Frank, M.G., 2013. Visual experience and subsequent sleep induce sequential plastic changes in putative inhibitory and excitatory cortical neurons. Proc. Natl. Acad. Sci. U. S. A. 110, 3101–3106. https://doi.org/10.1073/pnas.1208093110.

Averkin, R.G., Szemenyei, V., Bordé, S., Tamás, G., 2016. Identified cellular correlates of neocortical ripple and high-gamma oscillations during spindles of natural sleep. Neuron 92, 916–928. https://doi.org/10.1016/j.neuron.2016.09.032.

Azzam, D., Ronquillo, Y., 2023. Snellen Chart. Treasure Island (FL).

Barakat, M., Doyon, J., Debas, K., Vandewalle, G., Morin, A., Poirier, G., Martin, N., Lafortune, M., Karni, A., Ungerleider, L.G., Benali, H., Carrier, J., 2011. Fast and slow spindle involvement in the consolidation of a new motor sequence. Behav. Brain Res. 217, 117–121. https://doi.org/10.1016/j.bbr.2010.10.019.

Bates, D., Mächler, M., Bolker, B., Walker, S., 2015. Fitting linear mixed-effects models using lme4. J. Stat. Softw. 67, 1–48. https://doi.org/10.18637/jss.v067.i01.

Berry, R., Quan, S., Abreu, A., Bibbs, M., DelRosso, L., Harding, S., Mao, M., Plante, D., Pressman, M., Troester, M., Vaughn, B., Darien, I.L., 2020. The AASM Manual for the Scoring of Sleep and Associated Events: Rules, Terminology and Technical Specifications, Version 2. America Academy of Sleep Medicine, Darien, IL.

Bhardwaj, R.D., Curtis, M.A., Spalding, K.L., Buchholz, B.A., Fink, D., Björk-Eriksson, T., Nordborg, C., Gage, F.H., Druid, H., Eriksson, P.S., Frisén, J., 2006. Neocortical neurogenesis in humans is restricted to development. Proc. Natl. Acad. Sci. U. S. A. 103, 12564–12568. https://doi.org/10.1073/pnas.0605177103.

Bollini, A., Cocchi, E., Salvagno, V., Gori, M., 2023. The causal role of vision in the development of spatial coordinates: evidence from visually impaired children. J. Exp. Psychol. Hum. Percept. Perform. https://doi.org/10.1037/xhp0001122.

Campbell, I.G., Feinberg, I., 2016. Maturational patterns of sigma frequency power across childhood and adolescence: a longitudinal study. Sleep 39, 193–201. https://doi.org/10.5665/sleep.5346.

Campus, C., Signorini, S., Vitali, H., De Giorgis, V., Papalia, G., Morelli, F., Gori, M., 2021. Sensitive period for the plasticity of alpha activity in humans. Dev. Cogn. Neurosci. 49, 100965 https://doi.org/10.1016/j.dcn.2021.100965.

Cao, J., Herman, A.B., West, G.B., Poe, G., Savage, V.M., 2020. Unraveling why we sleep: quantitative analysis reveals abrupt transition from neural reorganization to repair in early development. Sci. Adv. 6, 1–12. https://doi.org/10.1126/sciadv.aba0398.

Cappagli, G., Cocchi, E., Gori, M., 2017. Auditory and proprioceptive spatial impairments in blind children and adults. Dev. Sci. 20 https://doi.org/10.1111/desc.12374.

Cappagli, G., Finocchietti, S., Cocchi, E., Giammari, G., Zumiani, R., Cuppone, A.V., Baud-Bovy, G., Gori, M., 2019. Audio motor training improves mobility and spatial cognition in visually impaired children. Sci. Rep. 9, 1–9. https://doi.org/10.1038/s41598-019-39981-x.

Chatburn, A., Coussens, S., Lushington, K., Kennedy, D., Baumert, M., Kohler, M., 2013. Sleep spindle activity and cognitive performance in healthy children. Sleep 36, 237–243. https://doi.org/10.5665/sleep.2380.

Clemens, Z., Fabó, D., Halász, P., 2005. Overnight verbal memory retention correlates with the number of sleep spindles. Neuroscience 132, 529–535. https://doi.org/10.1016/j.neuroscience.2005.01.011.

Clemens, Z., Mölle, M., Eross, L., Jakus, R., Rásonyi, G., Halász, P., Born, J., 2011. Fine-tuned coupling between human parahippocampal ripples and sleep spindles. Eur. J. Neurosci. 33, 511–520. https://doi.org/10.1111/j.1460-9568.2010.07505.x.

D'Atri, A., Novelli, L., Ferrara, M., Bruni, O., De Gennaro, L., 2018. Different maturational changes of fast and slow sleep spindles in the first four years of life. Sleep Med 42, 73–82. https://doi.org/10.1016/j.sleep.2017.11.1138.

Dale, N., Sakkalou, E., O'Reilly, M., Springall, C., De Haan, M., Salt, A., 2017. Functional vision and cognition in infants with congenital disorders of the peripheral visual system. Dev. Med. Child Neurol. 59, 725–731. https://doi.org/10.1111/dmcn.13429.

Doucette, M.R., Kurth, S., Chevalier, N., Munakata, Y., LeBourgeois, M.K., 2015. Topography of slow sigma power during sleep is associated with processing speed in preschool children. Brain Sci. 5, 494–508. https://doi.org/10.3390/brainsci5040494.

Drasgow, F., 2004. Polychoric and polyserial correlations. Encyclopedia of Statistical Sciences. John Wiley & Sons, Ltd. https://doi.org/10.1002/0471667196.ess2014.

Eisermann, M., Kaminska, A., Moutard, M.L., Soufflet, C., Plouin, P., 2013. Normal EEG in childhood: from neonates to adolescents. Neurophysiol. Clin. 43, 35–65. https://doi.org/10.1016/j.neucli.2012.09.091.

Fernandez, L.M.J., Lüthi, A., 2020. Sleep spindles: mechanisms and functions. Physiol. Rev. 100, 805–868. https://doi.org/10.1152/physrev.00042.2018.

Fifer, W.P., Byrd, D.L., Kaku, M., Eigsti, I.M., Isler, J.R., Grose-Fifer, J., Tarullo, A.R., Balsam, P.D., 2010. Newborn infants learn during sleep. Proc. Natl. Acad. Sci. U. S. A. 107, 10320–10323. https://doi.org/10.1073/pnas.1005061107.

Fogel, S.M., Smith, C.T., 2011. The function of the sleep spindle: a physiological index of intelligence and a mechanism for sleep-dependent memory consolidation. Neurosci. Biobehav. Rev. 35, 1154–1165. https://doi.org/10.1016/j.neubiorev.2010.12.003.

Fox, J., Weisberg, S., 2018. An R companion to Applied Regression. Sage publications.

Geiger, A., Huber, R., Kurth, S., Ringli, M., Jenni, O.G., Achermann, P., 2011. The sleep EEG as a marker of intellectual ability in school age children. Sleep 34, 181–189. https://doi.org/10.1093/sleep/34.2.181.

Gilmore, J.H., Knickmeyer, R.C., Gao, W., 2018. Imaging structural and functional brain development in early childhood. Nat. Rev. Neurosci. 19, 123–137. https://doi.org/10.1038/nrn.2018.1.

Gori, M., Campus, C., Signorini, S., Rivara, E., Bremner, A.J., 2021. Multisensory spatial perception in visually impaired infants. Curr. Biol. 31, 5093–5101. https://doi.org/10.1016/j.cub.2021.09.011 e5.

Grandchamp, R., Delorme, A., 2011. Single-trial normalization for event-related spectral decomposition reduces sensitivity to noisy trials. Front. Psychol. 2, 236. https://doi.org/10.3389/fpsyg.2011.00236.

Grigg-Damberger, M.M., Nevšímalová, S., Bruni, O., 2017. Ontogeny of sleep and its functions in infancy, childhood, and adolescence. Sleep Disorders in Children. Springer US, pp. 3–29.

Gruber, R., Wise, M.S., 2016. Sleep spindle characteristics in children with neurodevelopmental disorders and their relation to cognition. Neural Plast. 2016, 4724792 https://doi.org/10.1155/2016/4724792.

Gruber, R., Wise, M.S., Frenette, S., Knäauper, B., Boom, A., Fontil, L., Carrier, J., 2013. The association between sleep spindles and IQ in healthy school-age children. Int. J. Psychophysiol. Off. J. Int. Organ. Psychophysiol. 89, 229–240. https://doi.org/10.1016/j.ijpsycho.2013.03.018.

Guadagni, V., Byles, H., Tyndall, A.V., Parboosingh, J., Longman, R.S., Hogan, D.B., Hanly, P.J., Younes, M., Poulin, M.J., 2021. Association of sleep spindle characteristics with executive functioning in healthy sedentary middle-aged and older adults. J. Sleep Res. 30, e13037. https://doi.org/10.1111/jsr.13037.

Halassa, M.M., Kastner, S., 2017. Thalamic functions in distributed cognitive control. Nat. Neurosci. 20 https://doi.org/10.1038/s41593-017-0020-1.

Hoedlmoser, K., Heib, D.P.J., Roell, J., Peigneux, P., Sadeh, A., Gruber, G., Schabus, M., 2014. Slow sleep spindle activity, declarative memory, and general cognitive abilities in children. Sleep 37, 1501–1512. https://doi.org/10.5665/sleep.4000.

Houwen, S., Hartman, E., Visscher, C., 2009. Physical activity and motor skills in children with and without visual impairments. Med. Sci. Sports Exerc. 41, 103–109. https://doi.org/10.1249/MSS.0b013e318183389d.

Houwen, S., Visscher, C., Hartman, E., Lemmink, K.A.P.M., 2007. Gross motor skills and sports participation of children with visual impairments. Res. Q. Exerc. Sport 78, 16–23. https://doi.org/10.1080/02701367.2007.10762235.

Hyvarinen, L., Nasanen, R., Laurinen, P., 1980. New visual acuity test for pre-school children. Acta Ophthalmol. 58, 507–511. https://doi.org/10.1111/j.1755-3768.1980.tb08291.x.

Jaramillo, V., Schoch, S.F., Markovic, A., Kohler, M., Huber, R., Lustenberger, C., Kurth, S., 2023. An infant sleep electroencephalographic marker of thalamocortical connectivity predicts behavioral outcome in late infancy. Neuroimage 269, 119924. https://doi.org/10.1016/j.neuroimage.2023.119924.

Kurdziel, L., Duclos, K., Spencer, R.M.C., 2013. Sleep spindles in midday naps enhance learning in preschool children. Proc. Natl. Acad. Sci. 110, 17267LP–17272LP. https://doi.org/10.1073/pnas.1306418110.

Kwon, H., Walsh, K.G., Berja, E.D., Manoach, D.S., Eden, U.T., Kramer, M.A., Chu, C.J., 2023. Sleep spindles in the healthy brain from birth through 18 years. Sleep 46. https://doi.org/10.1093/sleep/zsad017.

Laventure, S., Pinsard, B., Lungu, O., Carrier, J., Fogel, S., Benali, H., Lina, J.M., Boutin, A., Doyon, J., 2018. Beyond spindles: interactions between sleep spindles

and boundary frequencies during cued reactivation of motor memory representations. Sleep 41. https://doi.org/10.1093/sleep/zsy142.

Lenth, R.V., 2022. emmeans: Estimated Marginal Means, aka Least-Squares Means. https://cran.r-project.org/web/packages/emmeans/emmeans.pdf.

Louis, J., Zhang, J.X., Revol, M., Debilly, G., Challamel, M.J., 1992. Ontogenesis of nocturnal organization of sleep spindles: a longitudinal study during the first 6 months of life. Electroencephalogr. Clin. Neurophysiol. 83, 289–296. https://doi.org/10.1016/0013-4694(92)90088-Y.

Lustenberger, C., Maric, A., Dürr, R., Achermann, P., Huber, R., 2012. Triangular relationship between sleep spindle activity, general cognitive ability and the efficiency of declarative learning. PLoS One 7. https://doi.org/10.1371/journal.pone.0049561.

MacLean, J.E., Fitzgerald, D.A., Waters, K.A., 2015. Developmental changes in sleep and breathing across infancy and childhood. Paediatr. Respir. Rev. 16, 276–284. https://doi.org/10.1016/j.prrv.2015.08.002.

Maquet, P., 2010. Understanding non rapid eye movement sleep through neuroimaging. World J. Biol. psychiatry Off. J. World Fed. Soc. Biol. Psychiatry 11 (Suppl 1), 9–15. https://doi.org/10.3109/15622971003637736.

McClain, I.J., Lustenberger, C., Achermann, P., Lassonde, J.M., Kurth, S., LeBourgeois, M.K., 2016a. Developmental changes in sleep spindle characteristics and sigma power across early childhood. Neural Plast. 2016, 1–9. https://doi.org/10.1155/2016/3670951.

McClain, I.J., Lustenberger, C., Achermann, P., Lassonde, J.M., Kurth, S., LeBourgeois, M.K., 2016b. Developmental changes in sleep spindle characteristics and sigma power across early childhood. Neural Plast. 2016, 3670951 https://doi.org/10.1155/2016/3670951.

Menicucci, D., Lunghi, C., Zaccaro, A., Morrone, M.C., Gemignani, A., 2022. Mutual interaction between visual homeostatic plasticity and sleep in adult humans. eLife 11, e70633. https://doi.org/10.7554/eLife.70633.

Miller, A.L., Seifer, R., Crossin, R., Lebourgeois, M.K., 2015. Toddler's self-regulation strategies in a challenge context are nap-dependent. J. Sleep Res. 24, 279–287. https://doi.org/10.1111/jsr.12260.

Nobili, L., Ferrara, M., Moroni, F., De Gennaro, L., Russo, G.Lo, Campus, C., Cardinale, F., De Carli, F., 2011. Dissociated wake-like and sleep-like electro-cortical activity during sleep. Neuroimage 58, 612–619. https://doi.org/10.1016/j.neuroimage.2011.06.032.

Page, J., Lustenberger, C., Fröhlich, F., 2018. Social, motor, and cognitive development through the lens of sleep network dynamics in infants and toddlers between 12 and 30 months of age. Sleep 41. https://doi.org/10.1093/sleep/zsy024.

Piantoni, G., Poil, S.S., Linkenkaer-Hansen, K., Verweij, I.M., Ramautar, J.R., Van Someren, E.J.W., Van Der Werf, Y.D., 2013. Individual differences in white matter diffusion affect sleep oscillations. J. Neurosci. Off. J. Soc. Neurosci. 33, 227–233. https://doi.org/10.1523/JNEUROSCI.2030-12.2013.

Presaghi, F., Desimoni, M., 2023. random.polychor.pa: a parallel analysis with polychoric correlation matrices. R package version 1.1.4–3.

R Core Team, 2021. R: a language and environment for statistical computing. R Foundation for Statistical Computing, Vienna. https://www.R-project.org.

Rapoport, J.L., Castellanos, F.X., Gogate, N., Janson, K., Kohler, S., Nelson, P., 2001. Imaging normal and abnormal brain development: new perspectives for child psychiatry. Aust. N. Z. J. Psychiatry 35, 272–281. https://doi.org/10.1046/j.1440-1614.2001.00900.x.

Ray, L.B., Sockeel, S., Soon, M., Bore, A., Myhr, A., Stojanoski, B., Cusack, R., Owen, A.M., Doyon, J., Fogel, S.M., 2015. Expert and crowd-sourced validation of an individualized sleep spindle detection method employing complex demodulation and individualized normalization. Front. Hum. Neurosci. 9, 507. https://doi.org/10.3389/fnhum.2015.00507.

Revelle, W., 2009. An Introduction to Psychometric Theory with Applications in R. Springer. http://personality-project.org/r/book.

Revelle, W., 2016. psych: Procedures for Personality and Psychological Research. R package version 1.6.12. http://personality-project.org/r, http://personality-project.org/r/psych-manual.pdf.

Reynell, J., 1978. Developmental patterns of visually handicapped children. Child. Care. Health Dev. 4, 291–303.

Ricci, A., He, F., Calhoun, S.L., Fang, J., Vgontzas, A.N., Liao, D., Bixler, E.O., Younes, M., Fernandez-Mendoza, J., 2021. Sex and pubertal differences in the maturational trajectories of sleep spindles in the transition from childhood to adolescence: a population-based study. eNeuro 8. https://doi.org/10.1523/ENEURO.0257-21.2021.

Rigato, S., Begum Ali, J., Van Velzen, J., Bremner, A.J., 2014. The neural basis of somatosensory remapping develops in human infancy. Curr. Biol. 24, 1222–1226. https://doi.org/10.1016/j.cub.2014.04.004.

Sadeh, A., Gruber, R., Raviv, A., 2002. Sleep, neurobehavioral functioning, and behavior problems in school-age children. Child Dev. 73, 405–417. https://doi.org/10.1111/1467-8624.00414.

Sanai, N., Nguyen, T., Ihrie, R.A., Mirzadeh, Z., Tsai, H.H., Wong, M., Gupta, N., Berger, M.S., Huang, E., Garcia-Verdugo, J.M., Rowitch, D.H., Alvarez-Buylla, A., 2011. Corridors of migrating neurons in the human brain and their decline during infancy. Nature 478, 382–386. https://doi.org/10.1038/nature10487.

Sankupellay, M., Wilson, S., Heussler, H.S., Parsley, C., Yuill, M., Dakin, C., 2011. Characteristics of sleep EEG power spectra in healthy infants in the first two years of life. Clin. Neurophysiol. Off. J. Int. Fed. Clin. Neurophysiol. 122, 236–243. https://doi.org/10.1016/j.clinph.2010.06.030.

Schabus, M., Dang-Vu, T.T., Albouy, G., Balteau, E., Boly, M., Carrier, J., Darsaud, A., Degueldre, C., Desseilles, M., Gais, S., Phillips, C., Rauchs, G., Schnakers, C., Sterpenich, V., Vandewalle, G., Luxen, A., Maquet, P., 2007. Hemodynamic cerebral correlates of sleep spindles during human non-rapid eye movement sleep. Proc. Natl. Acad. Sci. U. S. A. 104, 13164–13169. https://doi.org/10.1073/pnas.0703084104.

Schoch, S.F., Jaramillo, V., Markovic, A., Huber, R., Kohler, M., Jenni, O.G., Lustenberger, C., Kurth, S., 2021. Bedtime to the brain: how infants sleep habits intertwine with sleep neurophysiology. bioRxiv. https://doi.org/10.1101/2021.11.08.467800.

Scholle, S., Zwacka, G., Scholle, H.C., 2007. Sleep spindle evolution from infancy to adolescence. Clin. Neurophysiol. 118, 1525–1531. https://doi.org/10.1016/j.clinph.2007.03.007.

Seibt, J., Richard, C.J., Sigl-Glöckner, J., Takahashi, N., Kaplan, D.I., Doron, G., De Limoges, D., Bocklisch, C., Larkum, M.E., 2017. Cortical dendritic activity correlates with spindle-rich oscillations during sleep in rodents. Nat. Commun. 8, 1–12. https://doi.org/10.1038/s41467-017-00735-w.

Shinomiya, S., Nagata, K., Takahashi, K., Masumura, T., 1999. Development of sleep spindles in young children and adolescents. Clin. Electroencephalogr. 30, 39–43. https://doi.org/10.1177/155005949903000203.

Sokoloff, G., Dooley, J.C., Glanz, R.M., Wen, R.Y., Hickerson, M.M., Evans, L.G., Laughlin, H.M., Apfelbaum, K.S., Blumberg, M.S., 2021. Twitches emerge postnatally during quiet sleep in human infants and are synchronized with sleep spindles. Curr. Biol. 31, 3426–3432. https://doi.org/10.1016/j.cub.2021.05.038 e4.

Steriade, M., 1999. Brainstem activation of thalamocortical systems. Brain Res. Bull. 50, 391–392. https://doi.org/10.1016/s0361-9230(99)00119-7.

Steriade, M., Deschênes, M., Domich, L., Mulle, C., 1985. Abolition of spindle oscillations in thalamic neurons disconnected from nucleus reticularis thalami. J. Neurophysiol. 54, 1473–1497. https://doi.org/10.1152/jn.1985.54.6.1473.

Tamaki, M., Matsuoka, T., Nittono, H., Hori, T., 2008. Fast sleep spindle (13-15 hz) activity correlates with sleep-dependent improvement in visuomotor performance. Sleep 31, 204–211. https://doi.org/10.1093/sleep/31.2.204.

Tarokh, L., Carskadon, M.A., Achermann, P., 2014. Early adolescent cognitive gains are marked by increased sleep EEG coherence. PLoS One 9, 1–5. https://doi.org/10.1371/journal.pone.0106847.

Tononi, G., Cirelli, C., 2014. Sleep and the price of plasticity: from synaptic and cellular homeostasis to memory consolidation and integration. Neuron 81, 12–34. https://doi.org/10.1016/j.neuron.2013.12.025.

Ujma, P.P., Sándor, P., Szakadát, S., Gombos, F., Bódizs, R., 2016. Sleep spindles and intelligence in early childhood-developmental and trait-dependent aspects. Dev. Psychol. 52, 2118–2129. https://doi.org/10.1037/dev0000233.

Vitali, H., Campus, C., De Giorgis, V., Signorini, S., Gori, M., 2022. The vision of dreams: from ontogeny to dream engineering in blindness. J. Clin. sleep Med. JCSM Off. Publ. Am. Acad. Sleep Med. 18, 2051–2062. https://doi.org/10.5664/jcsm.10026.

Wechsler, D., 2003. Wechsler intelligence scale for children, Fourth edition (WISC-IV. Tx: The psychological corporation, San Antonio. https://doi.org/10.1177/0734282906288389.